Monitoring Induced Currents on Long Conductive Structures During MRI

R. D. Venook[1,2], W. R. Overall[1], K. Shultz[1], S. Conolly[3], J. M. Pauly[1], and G. C. Scott[1]

[1]Electrical Engineering, Stanford University, Stanford, CA, United States, [2]Boston Scientific, Burlingame, CA, United States, [3]Bioengineering, U.C. Berkeley, Berkeley, CA, United States

Introduction Minimally invasive procedures, such as catheter-based stent delivery and ablation, have revolutionized surgical care. MRI-based guidance techniques could significantly improve the safety and effectiveness of many of these methods [1,2]. Unfortunately, because of the risk of RF heating, clinical application of these interventional MRI techniques remains limited. Similar heating concerns, including accounts of serious injury as a result of such heating, also contraindicate MRI for the rapidly growing number of patients with implanted deep brain stimulation (DBS) and cardiac pacemaker and defibrillation devices [3,4]. Prior work establishes the dangerous and resonant nature of heating near long conductive structures under MRI [5,6]. Such conductive structures remain a clinical or a practical necessity for many patients, however, and their presence in an MRI environment raises a risk of RF-induced heating that is both significant and unknown. A need exists for methods to mitigate and/or monitor this risk. This abstract presents an image-based analysis method for quantifying induced RF currents and their relation to the bioheat equation for spherical contact heating.

Measuring Current and with Image Artifacts Graf, et al. have reported observations about RF enhancement artifacts near metal objects under MRI, with some analysis of flip-angle distortions and geometric variation with scan parameters [7,8]. For induced RF currents on long, thin, and axially-oriented conductors, we observe 1) currents on thin structures create azimuthal magnetic fields; 2) magnetic fields at the Larmor frequency alter local flip angles during signal excitation; and 3) induced currents at the Larmor frequency alter local receiver sensitivity during signal reception. For a simple, axial current, the signal intensity artifact |S|, wire induced receive distortion B_{WR} and transmit field distortion B_{WT} augment B_1 as follows:

$$|S| = \left|(B_{wR} + B_{1R})\sin\left(\beta\left|B_{wT} + B_{1T}\right|\right)\right| \qquad B_{wR} = j\exp(j[\alpha+\phi])\mu_o I/4\pi r \qquad B_{wT} = -j\exp(j[\alpha-\phi])\mu_o I/4\pi r$$

Here, α is the phase offset of the current in the wire at the plane of interest, ϕ is the angular position in that axial plane, r is radial distance from wire center and β is a scalar that relates applied field to flip angle and depends upon RF pulse shape and duration. R and T refer to the circular polarization for receive and transmit in phasor form.

Methods& Results We performed wire artifact imaging studies in a large aqueous phantom (lwh=85x45x33cm) using a 160 cm long wire. We imaged with gradient echo sequences (echo time = 7 ms) on a 1.5 T scanner (GE Signa) with 15 and 60 degree flip angles. The simulations involved three parameters: the magnitude and phase of a complex scaling factor for artifact character, and a geometrical angle for orientation. Figures 1 and 2 display, alongside cropped images, simulated images of the artifact expected near an axial wire using the formulas above. The flip angles in the actual images (Figs. 1 and 2, left) differed by a factor of four. Because the coupling phase and geometry are invariant to flip angle, we verified the simulation method by scaling the 15° results a factor of four to validate with the 60° image data and simulations.

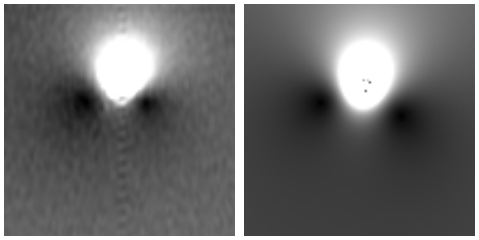

Figure 1: Artifact as measured (left) and simulated (right) for 15 degree flip angle.

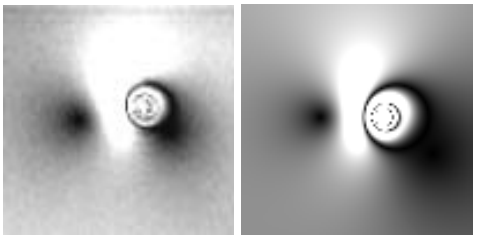

Figure 2: Artifact as measured (left) and simulated (right) with a 60° nominal flip angle. Simulation distortions simply scale with flip angle.

Discussion An important issue is translating current measurements from field distortion into heating. If current is converted to rms form, the nutation frequency a distance r from a wire is $F_T = 6 * I_{rms}/r$ Hz. A wire carrying 20 mA rms must produce a 120 Hz nutation or 2 ms 90° pulse 1 mm away. Indeed, for a spherical contact fed by an insulated wire (Fig. 3), it is easy to solve for the steady state heat increase:

$$\Delta T(r) = \frac{I_{rms}^2}{16\pi^2 \sigma k R_o}\left[\frac{1}{r} - \frac{R_o}{2r^2}\right]$$

Here k=0.5W/Cm and σ = 0.5s/m are typical tissue thermal and electrical conductivities, with zero perfusion and no heat flow into the contact. This worst case situation predicts for a Ro=1mm sphere radius only a 5°C steady state temperature rise at r=Ro. These levels are difficult to determine by MR thermometry but must produce obvious artifacts in feed-wires in MRI. This simple analysis also suggests device makers should assign a heating index based on electromagnetic contact geometry for unit injected current. The MRI manufacturer could then develop B1 mapping sequences that detect critical wire currents in pre-scan. This would replace the nebulous dependence on SAR levels. In fact, a RF field mapping approach [9] (Fig. 4) could further aid in quantifying lead properties.

Conclusion A simple model for image artifacts due to axial RF-induced currents was developed. Future extensions include arbitrary orientations. Combined with a parameter estimation routine, this model can enable detection of the coupling between a transmitter and an internal conductive structure without affecting the electromagnetic environment. In general these results suggest that B1 mapping techniques can quantifiably detect unsafe RF conditions and be used to assess implanted lead performance within an MRI environment.

References

[1] Bakker CJ, et al., J MRI 1998; 8:245–250. [2] Eggebrecht H, et al., Eur Heart Journal 2006; 27:613–620. [3] Rezai AR, et al., Invest Radiol 2004; 39:300–303. [4] Nyenhuis JA, et al., IEEE Trans Dev Mat Rel 2005; 5:467–80. [5] Konings MK, et al., J Magn Reson Imaging 2000; 12:79–85. [6] Nitz WR, et al., J Magn Reson Imaging 2001; 13:105–114. [7] Graf H, et al., Magn Reson Imaging 2005; 23:493–9. [8] Graf H, et al., Med Phys 2006; 33:124–127.[9] Scott G, et al., 13th ISMRM, p.151, 2005.

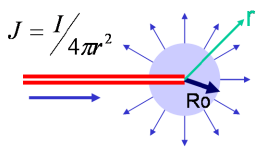

Figure 3: Spherical contact geometry for heat rise.

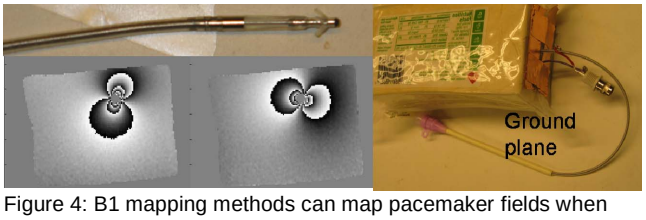

Figure 4: B1 mapping methods can map pacemaker fields when driven as monopoles to assess RF insulating ability and contact current crowding. (lead courtesy J Meador, Medtronic).

Acknowledgements We gratefully acknowledge the support of the following grants: NIH R33 CA1182756, NIH R01 EB008108, NIH R21 EB007715